Evidence for Differential Binding of Isoniazid by *Mycobacterium tuberculosis* KatG and the Isoniazid-Resistant Mutant KatG(S315T)

Nancy L. Wengenack,[‡] Smilja Todorovic,[‡,§] Lian Yu,[‡] and Frank Rusnak*[,‡]

Section of Hematology Research, Department of Biochemistry and Molecular Biology, Mayo Clinic, Rochester, Minnesota 55905, and Faculty of Physical Chemistry, University of Belgrade, Belgrade, Yugoslavia

Received August 21, 1998; Revised Manuscript Received September 8, 1998

ABSTRACT: Isoniazid is a mainstay of antibiotic therapy for the treatment of tuberculosis, but its molecular mechanism of action is unclear. Previous investigators have hypothesized that isoniazid is a prodrug that requires in vivo activation by KatG, the catalase−peroxidase of *Mycobacterium tuberculosis*, and that resistance to isoniazid strongly correlates with deletions or point mutations in KatG. One such mutation, KatG(S315T), is found in approximately 50% of clinical isolates exhibiting isoniazid resistance. In this work, ^{1}H nuclear magnetic resonance T_1 relaxation measurements indicate that KatG and KatG(S315T) each bind isoniazid at a position ≈12 Å from the active site heme iron. Electron paramagnetic resonance spectroscopy revealed heterogeneous populations of high-spin ferric heme in both wild-type KatG and KatG(S315T) with the ratios of each species differing between the two enzymes. Small changes in the proportions of these high-spin species upon addition of isoniazid support the finding that isoniazid binds near the heme periphery of both enzymes. Titration of wild-type KatG with isoniazid resulted in the appearance of a "type I" substrate-induced difference spectrum analogous to those seen upon substrate binding to the cytochromes P_{450}. The difference spectrum may result from an isoniazid-induced change in a portion of the KatG heme iron from 6- to 5-coordinate. Titration of KatG(S315T) with isoniazid failed to produce a measurable difference spectrum indicating an altered active site configuration. These results suggest that KatG(S315T) confers resistance to isoniazid through subtle changes in the isoniazid binding site.

According to the latest World Health Organization report, infectious diseases are the leading cause of death worldwide with 16.4 million people per year succumbing to the effects of virulent microbes (*1*). The age-old foe tuberculosis remains responsible for 3.1 million deaths per year accounting for approximately 19% of all deaths due to infectious disease and making tuberculosis the largest single killer among the infectious diseases (*1*).

One of the most successful antibiotics used to treat tuberculosis is isoniazid (isonicotinic acid hydrazide, Table 1), which was first utilized in clinical trials in 1951 and continues to be a mainstay of combination antibiotic therapy (*2*). Given isoniazid's long history of clinical use, it is surprising that many questions remain regarding its exact mechanism of action. Recent work has indicated that isoniazid is a prodrug that requires activation in vivo by KatG, the catalase−peroxidase of *Mycobacterium tuberculosis*. Zhang et al. demonstrated that KatG plays a vital role in potentiating isoniazid's efficacy when they restored isoniazid sensitivity to previously resistant strains of *M. tuberculosis* through the introduction of functional, plasmid-borne *katG* (*3*, *4*). Subsequent studies have demonstrated that isoniazid acts as an inhibitor of key mycobacterial enzymes involved in mycolic acid synthesis. Mycolic acids are extremely long-chained (C_{70}−C_{90}) fatty acids, unique to mycobacteria, that impart a significant permeability barrier to the cell wall (*5*). Enzymes involved in mycolic acid synthesis that are inhibited by activated isoniazid include InhA, the enoyl-ACP reductase of *M. smegmatis*, and a β-ketoacyl ACP synthase of *M. tuberculosis* (*6*−*8*). However, inhibition of these enzymes occurs only in the presence of functional KatG, suggesting that isoniazid is a prodrug requiring in vivo activation (*9*). Recently Rozwarski et al. characterized an adduct of activated isoniazid with NAD^+ [1] at the active site of InhA, reinforcing the hypothesis that isoniazid requires activation (*10*). The identity of the activated form of isoniazid remains unknown and is the subject of great scientific interest. None of the known, stable oxidation products of isoniazid have demonstrated antimycobacterial activity, suggesting that a reactive intermediate (e.g., an acyl anion or radical) is responsible for inhibition of enzymes involved in mycolic acid synthesis (*9*).

KatG is a homodimer of 82 kDa subunits, each of which binds a single iron−protoporphyrin IX cofactor (*11*). Interestingly, KatG is capable of catalyzing several reactions. Initial purification and characterization of KatG from *M. smegmatis* and *M. tuberculosis* revealed both catalase and peroxidase activities and led to speculation that isoniazid may

* Corresponding Author. Telephone: (507)284-4743. Fax: (507)-284-8286. E-mail: rusnak@mayo.edu.

‡ Mayo Clinic.

§ University of Belgrade.

[1] Abbreviations: CN, cyanide; CCP, cytochrome *c* peroxidase; EPR, electron paramagnetic resonance; MIC, minimal inhibitory concentration; NAD, nicotinamide adenine dinucleotide; NMR, nuclear magnetic resonance.

10.1021/bi982023k CCC: $15.00
Published on Web 10/22/1998

be activated through a traditional catalase−peroxidase compound I/compound II pathway (*9*, *11*−*14*). Since that time, several other enzymatic activities have been associated with KatG. The first is a Mn(II)-dependent peroxidase activity analogous to the activity of manganese peroxidase isolated from the white rot fungus *Phanerochaete chrysosporium* (*15*, *16*). In addition, a cytochrome P_{450}-like monooxygenase activity has also been described (*17*). Furthermore, superoxide has recently been demonstrated to enhance isoniazid- and KatG-dependent inhibition of *M. tuberculosis* colony formation, and it was suggested that superoxide (via KatG activation) may be responsible for isoniazid oxidation to a reactive intermediate (*18*). The presence of these diverse activities within a single enzyme has made identification of the activated form of isoniazid even more difficult since it is now unclear which activity or activities are utilized by KatG in the activation of isoniazid.

The emergence of isoniazid-resistant strains of *M. tuberculosis* has placed renewed emphasis on understanding the biochemical basis of isoniazid's antimycobacterial action and the role played by KatG in activating this clinically important antibiotic. We believe that insight into the mechanisms of isoniazid activation and resistance may be gained from the study of naturally occurring KatG mutants. Clinical isolates of *M. tuberculosis* that are resistant to isoniazid show a strong correlation with a KatG mutation in which serine at amino acid residue 315 is changed to threonine [KatG(S315T)] (*19*−*21*). Analysis of the *katG* sequence from isoniazid-resistant *M. tuberculosis* clinical isolates has demonstrated that KatG(S315T) correlates with resistance in >50% of the isolates examined and confers an 80-fold increase in the MIC for isoniazid (*20*−*22*). We have previously demonstrated that this mutation has significant effects on the ability of KatG to convert isoniazid to isonicotinic acid in vitro (*23*). As such, we were interested in delineating the basis for KatG(S315T)'s reduced ability to turn over isoniazid. In this work, we provide spectroscopic data demonstrating that isoniazid binds both wild-type KatG and KatG(S315T). ^{1}H NMR T_1 relaxation measurements allowed for estimation of the distance between isoniazid aromatic protons and the active site iron for both enzymes. In addition, the effect of isoniazid on the optical and EPR properties of wild-type KatG are reported and contrasted with those of KatG(S315T). The data are consistent with subtle alteration of isoniazid binding by KatG(S315T) as compared to wild-type KatG.

MATERIALS AND METHODS

Chemicals. Sodium cyanide was purchased from EM Science (Gibbstown, NJ). Tris and sodium phosphate were purchased from Curtin Matheson Scientific (Houston, TX). Isoniazid was purchased from Sigma Chemical Co. and recrystallized from boiling methanol using activated charcoal decolorization and hot filtration through Whatman no. 1 filter paper (Whatman International Ltd, Maidstone, U.K.). The crystals were vacuum filtered, washed with ice-cold methanol, and air-dried yielding white needles with a melting point of 172 °C.

Hazardous Procedures. Sodium cyanide is highly toxic and should be handled with caution using appropriate safety equipment and in accordance with the manufacturer's Material Safety Data Sheet.

Protein Preparation. Overexpression and purification of recombinant *M. tuberculosis* wild-type KatG and KatG(S315T) proteins from *Escherichia coli* has been previously described (*23*). Protein concentrations were determined using the Pierce (Rockford, IL) Coomassie plus protein reagent with bovine serum albumin as the standard (*24*).

Optical Spectroscopy. Spectra were recorded in 50 mM sodium phosphate buffer (pH 7.5) using a Cary 1 dual-beam spectrophotometer equipped with jacketed cuvette holders. Optical difference spectra were obtained at 37 °C in 50 mM sodium phosphate buffer (pH 7.5) using identical concentrations of enzyme (6 μM) in both the sample and reference cuvettes. The titrations were conducted by adding 1-μL aliquots of isoniazid or sodium cyanide stock solutions (prepared in 50 mM sodium phosphate buffer, pH 7.5) to the sample cuvette. The enzyme in the reference cell was diluted similarly using buffer. The solution in each cuvette was stirred continuously, and the difference spectra were recorded 1 min after each addition. Titrations were performed in triplicate.

Kinetic Analysis. Spectrophotometric determination of kinetic parameters was conducted in 50 mM sodium phosphate buffer (pH 7.5) at 37 °C by following *o*-dianisidine oxidation at 460 nm (ϵ_{460} = 11 300 M^{-1} cm^{-1}) in the presence of 25 mM *tert*-butylhydroperoxide (*14*). The isoniazid concentration was fixed at 20 μM, which is approximately 5 times the K_I reported for competitive inhibition of *M. smegmatis* KatG peroxidase activity by isoniazid (*14*). Double reciprocal plots were fit to eq 1, which describes competitive inhibition:

$$\frac{1}{v} = \frac{K_M\left(1 + \frac{[I]}{K_I}\right)}{V_{max}[S]} + \frac{1}{V_{max}} \quad (1)$$

where [S] and [I] are the *o*-dianisidine and isoniazid concentrations, respectively. Triplicate assays were conducted.

Electron Paramagnetic Resonance Spectroscopy. EPR spectra were obtained using a Bruker ESP300E spectrometer operating at X-band microwave frequency (9.45 GHz) and equipped with an Oxford Instruments ESR 900 continuous flow cryostat for temperature control. The spectra of wild-type KatG and KatG(S315T) (each 0.25 mM in 50 mM Tris-HCl, 150 mM NaCl, pH 8.0) were recorded under aerobic conditions at nonsaturating microwave power. The samples were then thawed at room temperature, and 2 equiv of isoniazid were added in a minimum volume of 50 mM sodium phosphate buffer (pH 7.5). The samples were mixed, placed on ice for 5 min to allow equilibration, frozen by immersion in liquid N_2, and the spectra were recorded. The fluoride complex was generated by the addition of excess (solid) sodium fluoride.

The experimental EPR spectra were obtained from the frozen solution, which can be regarded as equivalent to the powder spectra (i.e., averaged over the angle of oriented-crystal spectra). The spectra of high-spin ferric species can be interpreted in terms of the spin Hamiltonian, which for an iron ion in a noncubic crystal field has the form

$$\hat{H} = g\beta\vec{H}\vec{S} + D[S_z^2 + {}^1/_3S(S+1)] + E(S_x^2 - S_y^2) \quad (2)$$

where g is the intrinisic g value and is usually isotropic for high-spin ferric species, β is the Bohr magneton, $\vec{H}$ is the applied magnetic field, and D and E are the zero-field splitting parameters with D reflecting axial and E reflecting rhombic distortion from cubic symmetry. The simulations were performed using Bruker SimFonia software (version 1.2) for powder simulations. The energy of the microwave quantum at X-band frequency (E/hc = 0.31 cm^{-1}) is much smaller than the zero-field splitting in heme proteins (2 < D < 11 cm^{-1}), causing the EPR transitions to occur within each Kramers doublet and not between them (*25*, *26*). Hence the spin Hamiltonian can be written for every doublet in the simplified form:

$$\hat{H}' = \beta\vec{H}g'\vec{S}' \qquad (3)$$

Therefore, simulations were carried out for the system with the so-called "fictitious spin" being $S' = 1/2$ and g' representing an effective g tensor (g_{eff}) describing resonance positions along the principal axes of the D tensor. Only allowed transitions are simulated. These assumptions allow the calculation of the powder spectra to be done on the basis of solving the simplified spin Hamiltonian, which depends on the value of H and the orientation of H through the angles θ and φ by spherical integrations over the magnetic field orientations. The number of θ and φ values required for a particular simulation depends on the anisotropy of the spectra. If all interactions are axially symmetric, φ can be set to 1. An anisotropic line width tensor (σ_x, σ_y, σ_z), corresponding to line widths along the principal axis of the g tensor, was used in the simulation. Line shapes were obtained as combinations of Gaussian and Lorentzian lines. The ratio of a single species in a composite spectrum was determined as the double integration value of the specified resonance as compared with the double integration value for the entire complex spectrum.

HPLC Analysis of Isoniazid Turnover. The aerobic conversion of isoniazid to isonicotinic acid was determined by HPLC using a method described previously (*23*). Samples were analyzed in triplicate, and concentrations were determined relative to a nonenzymatic control solution of isoniazid in 50 mM sodium phosphate buffer (pH 7.5).

NMR Spectroscopy. Proton NMR was recorded on a Bruker AMX 500 MHz spectrometer. The proteins were exchanged into a 5 mM sodium phosphate deuterium oxide solution by repeated passages through a Centricon 30 concentrator (Amicon, Inc, Beverly, MA). Isoniazid solutions were prepared in D_2O. The total sample volume was 0.5 mL. All measurements were conducted under anerobic conditions to eliminate contributions to the relaxation mechanisms from oxygen and to prevent isoniazid turnover by the enzyme, which is an oxygen-dependent process (*15*). The sample temperature was maintained at 298 K except during temperature dependence studies. Longitudinal relaxation times (T_{1obs}) were determined using the inversion recovery method, which utilizes a 180°−τ−90° pulse sequence where τ is the interval between the 180° and 90° pulse. T_{1obs} was calculated from the observed spectra using the following equation:

$$M_z(t) - M_0 = [M_z(0) - M_0]\exp(-\tau/T_{1obs}) \qquad (4)$$

where $M_z(t)$ is the peak area following the 90° pulse at interval τ, M_0 is the peak area prior to the 180° pulse, $M_z(0)$ is the peak area at $t = 0$ following the 180° pulse (*27*). Eight scans were collected at each τ with a 30 s delay time. When the relaxation time of the isoniazid protons is observed in the presence of enzyme, T_{1obs} is considered to be the sum the bound and free components and can be expressed as

$$\frac{1}{T_{1obs}} = \left(\frac{1}{T_{1b}} - \frac{1}{T_{1f}}\right)\frac{E_0}{K_d + S_0} + \frac{1}{T_{1f}} \qquad (5)$$

where T_{1b} is the T_1 of isoniazid ring protons when bound to the enzyme; T_{1f} is T_1 of free isoniazid protons; E_0 and S_0 are the initial concentrations of enzyme and isoniazid, respectively; and K_d is the dissociation constant of the enzyme−isoniazid complex (*28*, *29*). In this case, $S_0 \gg K_d$, and therefore the value of K_d can be ignored in eq 5. Measurement of T_{1obs} as a function of protein or substrate concentration allows for estimation of T_{1b} by fitting to eq 5. In this work, T_{1b} was determined by varying the enzyme concentration from 10 to 280 μM while keeping the isoniazid concentration fixed at 10 mM. T_{1b} consists of a paramagnetic component (T_{1M}) and a diamagnetic component (T_{1d}). The diamagnetic contribution to the relaxation mechanisms was determined using the reduced KatG−carbon monoxide complex that was prepared according to the method of Marcinkeviciene et al. (*14*). Optical spectroscopy of the sample in the NMR tube was used to confirm the presence of the enzyme−CO complex prior to and following T_1 measurements. T_{1obs} was found to be identical for free isoniazid and isoniazid in the presence of the enzyme−CO complex, indicating that the diamagnetic contribution to the relaxation time was negligible. The value obtained from eq 5 for T_{1b} was therefore taken to be equal to T_{1M}.

The paramagnetic contribution to the relaxation time of the protons of bound isoniazid can be related to the distance from the heme iron by the following equation:

$$\frac{1}{T_{1M}} = \frac{2\gamma_I^2 g^2\beta^2 S(S+1)}{15r^6}\left(\frac{3\tau_c}{1+\omega_I^2\tau_c^2} + \frac{7\tau_c}{1+\omega_S^2\tau_c^2}\right) \qquad (6)$$

where γ_I is the nuclear gyromagnetic ratio, g is the isotropic electronic g factor, β is the Bohr magneton, S is the electronic spin, r is the metal-proton distance, τ_c is the effective correlation time of the dipolar interaction, ω_I is the nuclear Lamor precession frequency, and ω_S is the electron Lamor frequency (*29*−*31*). Assuming $\omega_I^2\tau_c^2 \ll 1$, $\omega_S^2\tau_c^2 \gg 1$, and $\tau_c = 5 \times 10^{-11}$ s, eq 6 can be reduced to (*29*, *32*−*34*)

$$r(\text{cm}) = (4.33 \times 10^{-41}T_{1M})^{1/6} \qquad (7)$$

RESULTS

Nuclear Magnetic Resonance Spectroscopy. Figure 1 shows a series of ^{1}H NMR spectra of 10 mM isoniazid following 180°−τ−90° pulse sequences of varying τ. The resonance centered at 7.76 ppm corresponds to the H_α protons (see Table 1) while the H_β protons appear at 8.74 ppm. T_{1M} values were calculated for each pair of equivalent isoniazid protons, and a summary of results is presented in Table 1. Use of eq 5 requires that the rate of substrate exchange between the bound and free state is rapid as compared to the spin−lattice relaxation times (*29*). The rate

Table 1: Paramagnetic T_1 Relaxation Times (T_{1M}) and Proton−Iron Distances (r) for Isoniazid Binding to WT KatG and KatG(S315T)

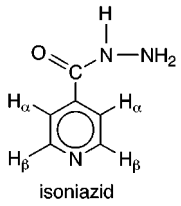

isoniazid

	proton	T_{1M} (s)	r (Å)
WT KatG	H_α	0.082 (± 0.03)	12 (± 2)
	H_β	0.074 (± 0.02)	12 (± 1)
KatG(S315T)	H_α	0.046 (± 0.003)	11 (± 0.1)
	H_β	0.033 (± 0.004)	11 (± 0.2)

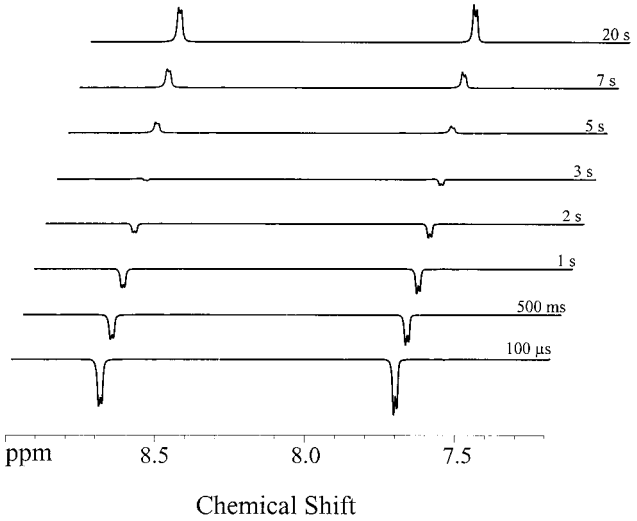

FIGURE 1: ^{1}H NMR T_{1obs} relaxation time measurements of isoniazid at 500 MHz. Spectra of 10 mM isoniazid in 5 mM sodium phosphate (pH 7.4)/D_2O at 25 °C obtained using a 180°−τ−90° pulse. Eight representative spectra are shown for clarity from a total of 14 τ values examined. Values used for τ ranged from 100 μs to 20 s and are indicated in the figure. The H_α protons (see Table 1) are represented by the doublet at 7.76 ppm, while the H_β protons resonate at 8.74 ppm.

of exchange was established by determining the temperature dependence of the relaxation time (T_{1obs}) for isoniazid in the presence of KatG(S315T). A linear increase in $1/T_{1obs}$ as a function of reciprocal temperature over the temperature range 283−303 K confirmed fast exchange. The presence of the paramagnetic center will effect the relaxation rate of bound isoniazid via dipolar mechanisms that depend on the distance to the iron atom. From the T_{1M} values, the distance to the heme iron was determined to be approximately 11−12 Å for each set of protons in *both* wild-type KatG and KatG(S315T). The symmetrical nature of the isoniazid ring protons does not allow a precise determination of the orientation of the molecule relative to the iron atom. However, these distances are compatible with a binding site for isoniazid at the heme periphery.

Optical Spectroscopy. The optical spectrum of wild-type KatG has a Soret maximum at 408 nm and α/β bands at approximately 530 and 630 nm, respectively (Figure 2A), and is essentially identical to the spectrum of *M. smegmatis* KatG (*14*). The addition of isoniazid to wild-type KatG resulted in a decreased Soret absorbance, a maximum shift to 406 nm, and a small but reproducible blue-shift in the

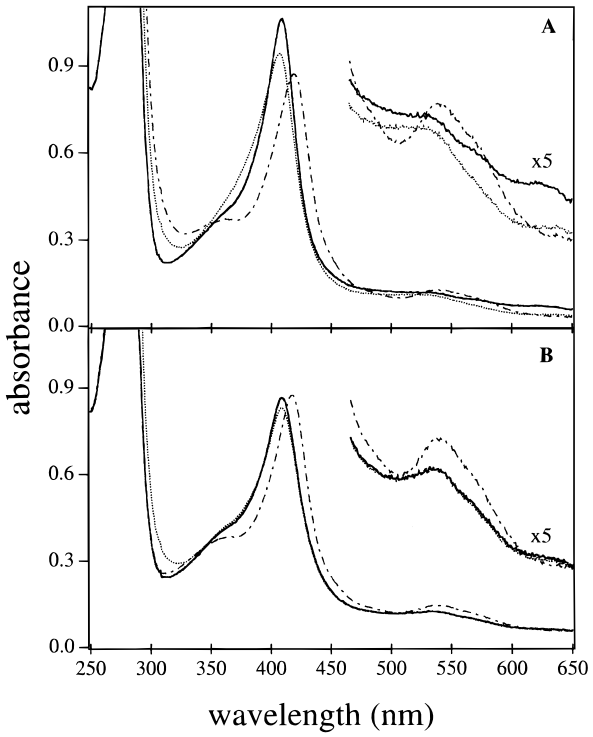

FIGURE 2: Optical absorption spectra of wild-type KatG (A) and KatG(S315T) (B) in 50 mM sodium phosphate buffer (pH 7.5) at 25 °C. (A) —, 10 μM wild-type KatG; ···, plus 0.50 mM isoniazid; — · —, plus 0.50 mM NaCN. (B) —, 10 μM KatG(S315T); ···, plus 1.0 mM isoniazid; — · —, plus 2.0 mM NaCN. The upper lines in each plot show the spectrum between 465 and 650 nm expanded 5-fold.

leading edge of the Soret band. The addition of cyanide to wild-type KatG caused a decreased Soret intensity, a red shift of the maximum to 419 nm, the appearance of a shoulder preceding the Soret at approximately 360 nm, and the appearance of α/β bands at approximately 540 nm. The shifts seen upon addition of cyanide are similar to other high-spin ferric heme proteins and are consistent with a conversion to a low-spin configuration about the heme iron (*35*, *36*).

In contrast, absorption spectra of KatG(S315T) differ from those of wild-type KatG. The KatG(S315T) Soret band maximum is at 409 nm, and α/β bands appear at approximately 535 nm (Figure 2B). The KatG(S315T) spectrum also has a distinct shoulder at about 360 nm that is more pronounced than in wild-type KatG. Addition of isoniazid to KatG(S315T) caused no change in the position of the Soret maximum but did cause a subtle decrease in its intensity. Contrary to its effect on wild-type KatG, addition of cyanide to KatG(S315T) caused no decrease in Soret intensity but red-shifted the maximum to 418 nm. A shoulder appears at 360 nm similar to that seen for the wild-type KatG−cyanide adduct, and the α/β maxima were also present at 537 nm. Since identical concentrations of enzyme were used to obtain each spectrum, the ϵ_{Soret} for KatG(S315T) appears to be lower than the ϵ_{Soret} for wild-type KatG. Further, the cyano adducts of both enzymes have identical ϵ values indicating equivalent amounts of iron were present in both enzymes following the spin conversion caused by cyanide.

Optical Difference Spectroscopy. The titration of 6 μM wild-type KatG with aliquots of isoniazid resulted in the appearance of a difference spectrum with sharp features in

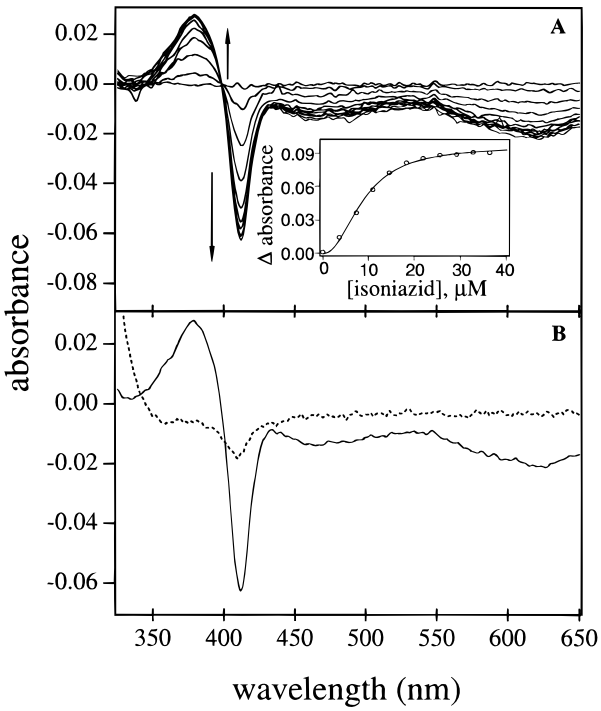

FIGURE 3: Optical difference spectra of wild-type KatG and KatG-(S315T) titrated with isoniazid. Titrations were conducted at 37 °C in 50 mM sodium phosphate buffer (pH 7.5). (A) 6 μM wild-type KatG titration with isoniazid (0−36 μM). The arrows indicate the direction of absorbance change upon addition of increasing amounts of isoniazid. The inset shows the titration progress monitored as the change in absorbance (peak absorbance at 378 nm minus the trough absorbance at 411 nm) as a function of isoniazid concentration. The data were fit to the Hill equation (n_{app} = 2.2, $[\text{isoniazid}]_{0.5}$ = 8.5 μM) using MacCurveFit version 1.3 (Kevin Raner Software Ltd., Victoria, Austrailia). (B) Isoniazid titration difference spectra of wild-type KatG vs KatG(S315T). —, wild-type KatG plus 36 μM isoniazid; - - -, KatG(S315T) plus 1.0 mM isoniazid. The increase in absorbance at < 350 nm is due to isoniazid absorbance.

the heme Soret region (Figure 3A). As the amount of isoniazid was increased to 36 μM, a peak with increasing intensity was noted at 380 nm, a trough occurred at 413 nm, and an isosbestic point was observed at 398 nm. A sigmoidal binding curve was obtained indicating positive cooperativity in isoniazid binding to the homodimer (inset, Figure 3A). Titration of 6 μM wild-type KatG with either 115 μM isonicotinic acid or 131 μM isonicotinamide, known stable products of isoniazid oxidation by KatG, failed to yield measurable difference spectra (data not shown). Titration of KatG(S315T) with isoniazid to a final concentration of 36 μM, an amount equivalent to that used in the titration of wild-type KatG, showed a featureless difference spectrum. Additional aliquots of isoniazid up to 1.0 mM resulted in only a small perturbation of the Soret region as shown in Figure 3B.

Titration of wild-type KatG with sodium cyanide to a final concentration of 15 μM resulted in the appearance of a difference spectrum with a trough at 404 nm and a peak at 426 nm (Figure 4A). Saturable binding was observed (inset, Figure 4A), and a single isosbestic point at 415 nm likely indicates the interconversion of two enzyme states. A similar titration of KatG(S315T) with cyanide resulted in a difference spectrum that is reminiscent of that seen for wild-type KatG with a trough at 404 nm and a peak at 424 nm (Figure 4B).

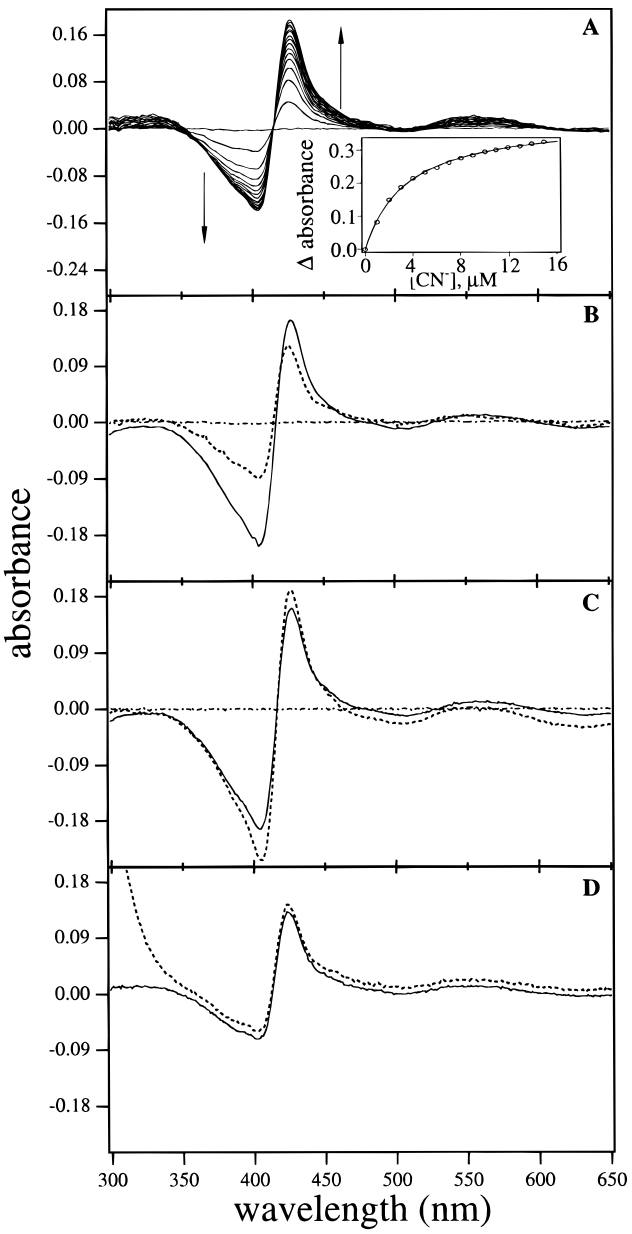

FIGURE 4: Optical difference spectra of wild-type KatG and KatG-(S315T) titrated with sodium cyanide. Titrations were conducted at 37 °C in 50 mM sodium phosphate buffer (pH 7.5). (A) 6 μM wild-type KatG titration with sodium cyanide (0−15 μM). The arrows indicate the direction of absorbance change upon addition of increasing amounts of cyanide. The inset shows the titration progress monitored as the change in absorbance (peak absorbance at 426 nm minus the trough absorbance at 404 nm) as a function of cyanide concentration. The data were fit to a binding isotherm ($n = 1$, $K_S = 3.5 \pm 0.1$ μM). (B) Cyanide titration difference spectra of wild-type KatG versus KatG(S315T). —, wild-type KatG plus 15 μM cyanide; - - -, KatG(S315T) plus 319 μM cyanide; — · —, control experiment conducted by titrating both the sample and reference cuvettes with equivalent aliquots of 50 mM sodium phosphate buffer (pH 7.5). The binding isotherm for the KatG-(S315T)−CN complex gave K_S = 2.3 ± 0.2 μM. (C) Double titration difference spectra of 6 μM wild-type KatG. —, wild-type KatG plus 15 μM cyanide; - - -, wild-type KatG plus 36 μM isoniazid then 15 μM cyanide. (D) Double titration difference spectra of 6 μM KatG(S315T). —, KatG(S315T) plus 319 μM cyanide; - - -, KatG(S315T) plus 1 mM isoniazid and then 319 μM cyanide (offset for viewing on the *y*-axis by +0.01 absorbance units). The increase in absorbance at <350 nm results from isoniazid absorbance.

The CN binding constant of KatG(S315T) was determined to be 2.3 ± 0.2 μM, nearly identical to that measured for CN binding to wild-type KatG (K_S = 3.5 ± 0.1 μM). The magnitude of the absorbance change following titration of KatG(S315T) with cyanide ($\Delta A_{peak - trough}$) was smaller than seen for wild-type KatG, but this difference would be predicted based on the differing ϵ_{Soret} values for wild-type KatG and KatG(S315T). A control titration showed no change the Soret region absorbance, confirming that the inflections seen upon addition of isoniazid and cyanide are the result of substrate- or ligand-induced alterations of the heme electronic configuration.

A dual titration of wild-type KatG with isoniazid followed by cyanide (or vice versa) resulted in a saturated type II difference spectrum of larger magnitude than that seen upon titrating with cyanide alone (Figure 4C, Table 2). Dual titration of KatG(S315T) with isoniazid followed by cyanide (or vice versa) resulted in a saturated type II difference spectrum of equal magnitude to that seen by titration with cyanide alone (Figure 4D, Table 2).

Kinetics. Isoniazid was found to be a competitive inhibitor of wild-type KatG peroxidase activity (versus *o*-dianisidine) with a K_I of 3.7 μM, which is in good agreement with the value obtained from the optical difference spectral titrations (Figure 3) and with the value reported previously for *M. smegmatis* KatG (K_I = 4.3 ± 0.7 μM) (*14*). Isoniazid was also found to be a competitive inhibitor (vs *o*-dianisidine) of KatG(S315T) peroxidase activity with K_I = 10.4 ± 1.1 μM.

Electron Paramagnetic Resonance Spectroscopy. The low-temperature EPR spectra of wild-type KatG and KatG-(S315T) in the presence and absence of isoniazid are shown in Figures 5 and 6, respectively. In addition, simulated spectra (Figures 5C,D and 6C,D) are presented that describe the individual species modeled to comprise the composite spectrum. The main species composing both the wild-type KatG and KatG(S315T) spectra have features at $g \sim 6$ and $g \sim 2$, which are indicative of high-spin ferric heme proteins. Weak features corresponding to a small amount of low-spin ferric species are also evident.

Powder simulations of wild-type KatG spectra show that the complex resonances that occur in the presence and absence of isoniazid can be modeled as a mixture of three distinct high-spin ferric species (Figure 5C,D). Each of these species are present in differing abundances as shown in Table 3. The most abundant species possesses near-axial symmetry with g_x = 5.57, g_y = 6.10, and $g_z \sim 2$. The second species has increased rhombic character with g_x = 5.08, g_y = 6.62, $g_z \sim 2$, and E/D = 0.03. The third species is a minor component that is purely axial with $g_\perp$ = 5.9, $g_{||} \sim 2$, and E/D = 0. Summation of these species according to the percentages noted in Table 3 yields composite simulated spectra that adequately represent the experimental spectra (e.g., compare Figure 5, panels B and C). Figure 7 demonstrates that addition of sodium fluoride to wild-type KatG converted all species into a single species with axial symmetry ($g_\perp$ = 6.0 and $g_{||}$ = 2.0). The presence of the fluoride in the coordination sphere of the iron is evident as hyperfine splitting due to interaction of the unpaired electronic spin of the iron with the nuclear magnetic moment of the ^{19}F nucleus, resulting in a doublet centered at $g_{||}$ = 2.0 with a coupling constant of 44 G.

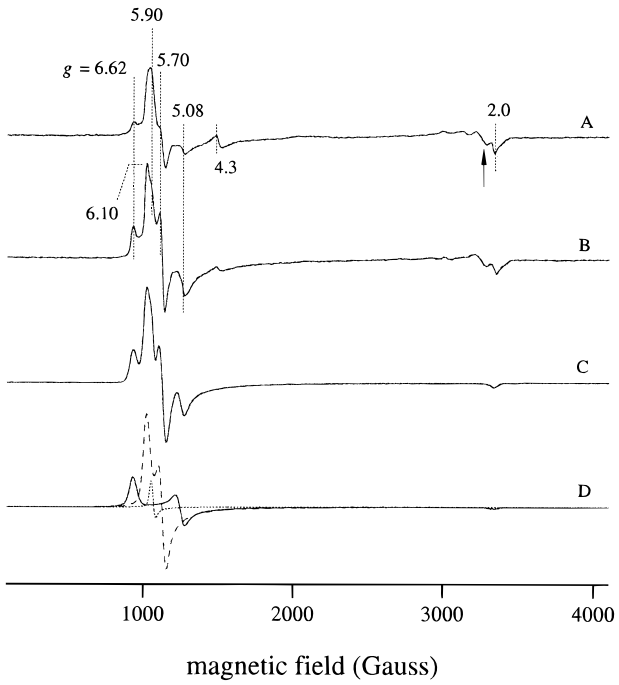

FIGURE 5: Low-temperature EPR spectra of wild-type KatG. (A) 250 μM wild-type KatG; (B) 250 μM wild-type KatG plus 2 equiv of isoniazid; (C) simulation of the spectrum shown in panel B using the components listed in Table 2; (D) component spectra of panel C calculated with the following parameters: —, species R, number of θ = 150, number of ϕ = 50, $\tilde{g}_{eff}$ = 6.62, 5.08, 2.0, and line width tensor σ = (46, 46, 46) G; - - -, species A1, number of θ = 200, number of ϕ = 50, $\tilde{g}_{eff}$ = 6.10, 5.57, 2.0, and σ = 20, 30, 20 G; •••, species A, number of θ = 150, number of ϕ = 1, $\tilde{g}_{eff}$ = 5.9, 5.9, 2.0, and σ = 40, 40, 40 G. Experimental conditions were as follows: microwave frequency, 9.45 GHz; modulation amplitude, 10 G; modulation frequency, 100 kHz; temperature, 4 K; and microwave power, 1 mW. The signal at g = 4.3 originates from a small amount of adventitious iron. A portion of the signal in the g = 2 region is due to a cavity contaminant (arrow, panel A).

The KatG(S315T) EPR spectrum can also be simulated as a mixture of the same three high-spin ferric species with the addition of a fourth, characteristic, rhombic species with g_x = 5.14, g_y = 6.30, and $g_z \sim 2$ (Figure 6C,D; Table 3). It should be mentioned that the fraction of the axial component (A) present in the spectrum of KatG(S315T) noted in Table 3 may be misleading. This resonance is significantly broadened in the mutant as compared to the wild type, often an indication of rhombic distortion. Therefore, the mutation does not necessarily lead to higher symmetry of the heme plane than in wild type, as it may appear from the percentage of axial species reported in Table 3.

The addition of isoniazid to either wild-type KatG or KatG(S315T) does not cause any new EPR signals to arise (Figures 5B and 6B). Rather, the distribution of the previously described components changes (Table 3). Upon addition of isoniazid, wild-type KatG experiences an increase in the percentage of components A1 and R at the expense of the purely axial component A, while KatG(S315T) experiences a decrease in components A and A1 with a corresponding increase in R and the unique component R1. Under the aerobic conditions used for preparation of the EPR samples, a portion of the isoniazid was converted to isonicotinic acid. The percentage of isoniazid remaining in each sample following EPR analysis was determined by HPLC, with 72 ± 5% isoniazid remaining in the wild-type

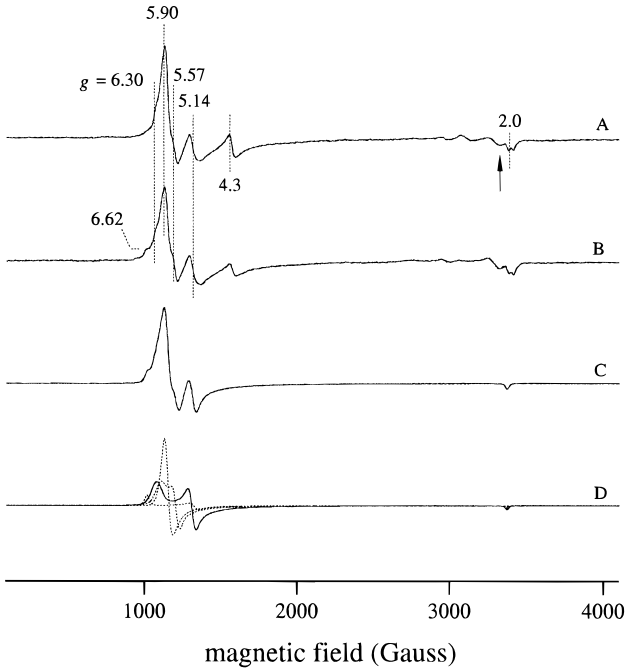

FIGURE 6: Low-temperature EPR spectra of KatG(S315T). (A) 250 μM KatG(S315T); (B) 250 μM KatG(S315T) plus 2 equiv of isoniazid; (C) simulation of the spectrum shown in panel B using the components listed in Table 2; (D) component spectra of panel C calculated with the following parameters: —, unique KatG(S315T) species R1, number of $\theta = 200$, number of $\phi = 100$, $\tilde{g}_{eff} = 6.30, 5.14, 2.0$, and line width tensor $\sigma = 22, 50, 20$ G; - - -, species A, A1, and R shown in wild-type KatG spectrum (Figure 5D). Experimental conditions were identical to those in Figure 5.

Table 2: Summary of Difference Spectra Magnitudes ($\Delta\epsilon$ Calculated from Peak minus Trough Heights)

substrate	KatG $\Delta\epsilon$ (M^{-1} cm^{-1})	KatG(S315T) $\Delta\epsilon$ (M^{-1} cm^{-1})
isoniazid	17 600 ± 1300	not detected
cyanide	55 600 ± 2800	34 500 ± 800
cyanide + isoniazid	67 600 ± 4000	34 300 ± 700
isoniazid + cyanide	64 300 ± 1900	35 500 ± 1900

KatG sample and 96 ± 0.3% isoniazid remaining in the KatG(S315T) sample.

DISCUSSION

Previous work in our laboratory has demonstrated that wild-type KatG is more efficient than the KatG(S315T) mutant in converting isoniazid to isonicotinic acid over a wide range of substrate concentrations even though both enzymes have similar catalase−peroxidase activities (*23*). In this work, comparison of the spectroscopic properties of wild-type KatG and the KatG(S315T) mutant reveal subtle differences in the active site configurations of the two enzymes in both the isoniazid-free and -bound states. As discussed below, these differences present two possible explanations for the reduced activation of isoniazid by KatG(S315T).

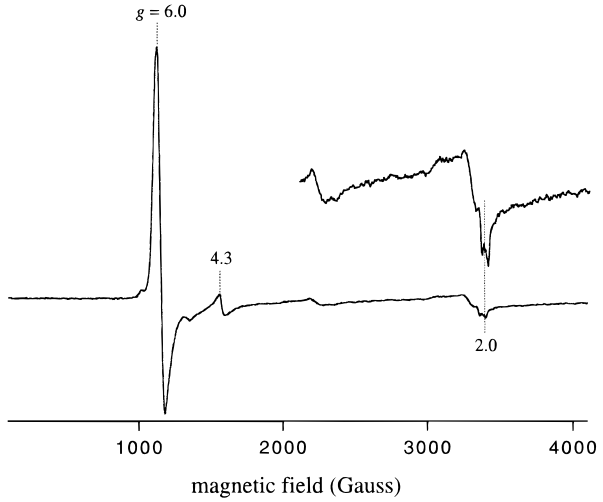

FIGURE 7: Low-temperature EPR spectra of wild-type KatG in the presence of excess sodium fluoride. Experimental conditions were identical to those in Figure 5. The upper line shows the doublet centered at $g_{||} = 2.0$ expanded 5-fold.

The optical spectrum of wild-type KatG is typical of *b*-type high-spin ferric hemoproteins such as metmyoglobin and cytochrome *c* peroxidase (CCP)[2] with a Soret maximum at 408 nm and α/β bands at 530 and 630 nm (*37, 38*). Consistent with this interpretation, the EPR spectrum of wild-type KatG, although heterogeneous, consists primarily of high-spin ferric species and is remarkably similar to the spectra reported previously for the catalase−peroxidase of *Streptomyces* sp. and the peroxidase of *Coprinus cinereus* (*39, 40*). Other investigators have also reported heterogeneity in the EPR spectrum of KatG isolated from various sources. Johnsson et al. found that recombinant *M. tuberculosis* KatG contained at least two rhombic high-spin ferric signals (*11*). The heterogeneity was attributed to a thermal equilibrium of spin configurations and the possible freezing-induced ligation of water or some active site ligand to the sixth coordination site of the iron. Marcinkeviciene et al. also reported that the EPR spectrum of *M. smegmatis* KatG exhibited a high-spin ferric signal with *g* values observed at 5.9 and 5.6 and attributed the small rhombic splitting to the presence of a six-coordinate heme iron containing water as the sixth ligand (*14*). The differences among the reported EPR spectra are not completely understood, but may in part be due to variable buffer conditions. For example, the EPR spectrum of *M. smegmatis* KatG was only observed following addition of ethylene glycol to the sample. Furthermore, buffer-dependent changes have been reported in EPR spectra

Table 3: Distribution of the High-Spin Ferric Species in Wild-Type KatG and KatG(S315T) in the Presence and Absence of Isoniazid[a]

	species			
sample	***A*** $g_{\perp} = 5.90$, $g_{||} \sim 2$ (%)	*A1* $\tilde{g}_{eff} = 6.10, 5.57, \sim 2$ (%)	*R* $\tilde{g}_{eff} = 6.62, 5.08, \sim 2$ (%)	*R1* $\tilde{g}_{eff} = 6.30, 5.14, \sim 2$ (%)
KatG	14	59	27	
KatG + isoniazid	3	64	33	
KatG(S315T)	42	30	< 1	28
KatG(S315T) + isoniazid	23	28	10	39

[a] Values represent the percentage of each species determined from the simulated spectra and are considered accurate to ± 7%.

of recombinant human ferric myoglobin mutants and cytochrome *c′* from *Rhodospiriuum rubrum* (*41*, *42*). Nevertheless, the high-spin species in wild-type KatG are interconvertible as demonstrated by the collapse to a single high-spin species with $g_{\perp} = 6.0$ and $g_{||} = 2.0$ upon formation of the fluoride complex. This result is consistent with that seen upon anion complex formation with the peroxidase of *C. cinereus* and *M. smegmatis* KatG (*40*, *14*). Furthermore, the fluoride anion is demonstrated to bind *M. tuberculosis* KatG at an axial position as evidenced by the hyperfine-split doublet at $g_{||} \approx 2.0$, an indication of fluoride binding to the heme iron (*43*). Despite the differences in heterogeneity, the EPR spectra from all sources agree that KatG contains primarily high-spin ferric heme, and computer simulation of the spectra allowed us to further delineate the complex signals arising from recombinant wild-type KatG. The component spectra consist of two species with rhombic character ($\tilde{g}_{\text{eff}} = 6.62$, 5.08, and 2.00, component R; and $\tilde{g}_{\text{eff}} = 6.10$, 5.57, and 2.00, component A1) and one species with axial character ($g_{\perp} = 5.90$ and $g_{||} = 2.00$, component A) (Table 3). The EPR spectra of high-spin, pentacoordinate peroxidases are frequently rhombic. For example, horseradish peroxidase exhibits *g* values of 6.35, 5.65, and 2.0 while the spectrum of CCP has *g* values of 6.4, 5.3, and 1.97 (*44*, *45*). Alternatively hexacoordinate, high-spin ferric hemoproteins usually show axial symmetry like that seen for metmyoglobin ($g_{\perp} = 6.0$ and $g_{||} = 2.0$) (*46*). The presence of both axial and rhombic signals in the wild-type KatG spectrum is consistent with the hypothesis that the recombinant enzyme exists as a mixture of 5- and 6-coordinate iron (*14*, *38*, *47*). As suggested by previous investigators, the sixth ligand may be contributed by water or some active site amino acid residue.

^{1}H NMR T_1 relaxation time measurements indicate that isoniazid binds wild-type KatG at a position ~12 Å from the heme iron providing the first report of proximity to the active site. For comparison, the terminal carboxylate oxygen of the heme propionates of yeast CCP are 8.5 Å from the heme iron.[3] Therefore, assuming similar active site configurations, these distances are consistent with isoniazid binding near the heme periphery. Further support for isoniazid binding near the heme is provided by the decreased Soret intensity and the appearance of a type I optical difference spectrum upon titration of wild-type KatG with isoniazid. Type I difference spectra have previously been reported for other hemoproteins following the binding of small substrates near the heme. Examples include binding of L-arginine to nitric oxide synthase, *p*-cresol to horseradish peroxidase, and aminopyrine to rat microsomal cytochrome P_{450} (*48*−*50*). A structural basis for type I spectra was recently provided by the crystal structure of the nitric oxide synthase oxidase domain, which confirmed binding of arginine near the heme (*51*). Type I difference spectra are normally associated with a low-to-high spin transition of the heme iron. However, low temperature EPR data and the room temperature optical spectrum with a Soret maximum at 408 nm indicate that KatG already exists in a predominantly high-spin configuration. While unusual, a type I optical difference spectrum resulting in a net retention of the high-spin character has precedence. For example, the binding of N^{G}-hydroxy-L-arginine to murine macrophage nitric oxide synthase resulted in a type I difference spectrum even though the enzyme was primarily high spin as isolated (*52*). Also, binding of substrates near the heme of hepatic microsomal cytochromes P_{450} has been associated with the alteration of a sixth ligand of the heme iron and the appearance of a type I difference spectrum (*53*). The difference spectrum obtained as a result of isoniazid binding to wild-type KatG may therefore reflect a conversion of a portion of the high-spin heme from 6- to 5-coordinate.

Titration of wild-type KatG with the strong-field ligand cyanide resulted in the expected type II difference spectrum, which is associated with a high-to-low spin transition of the heme iron. Dual titration of wild-type KatG with isoniazid followed by cyanide (or vice versa) resulted in a difference spectrum with increased magnitude (Δ absorbance = 0.40 ± 0.02) compared to titration with cyanide alone (Δ absorbance = 0.33 ± 0.02). These results provide further support for the idea that isoniazid alters the coordination state of (a portion of) the wild-type KatG heme iron as the increased magnitude can be explained by isoniazid-induced displacement of a sixth ligand that makes additional iron available for the cyanide-induced spin transition.

The EPR spectra following isoniazid addition to wild-type KatG show small changes in the intensities and distribution of various high-spin ferric species without the appearance of new components, supporting the hypothesis that isoniazid binds near the heme periphery of wild-type KatG. Under the conditions used to prepare the samples, some isoniazid turnover occurred; therefore, the EPR samples contain some of the products of isoniazid oxidation. However, HPLC analysis indicated that isoniazid was still the major species present. Further, titration of wild-type KatG with isonicotinic acid and isonicotinamide, two of the stable products of isoniazid oxidation, did not yield a measurable optical difference spectrum, implicating isoniazid as the source of heme perturbance in both the optical and EPR spectra. It is also interesting to note that isoniazid binding to wild-type KatG is cooperative (inset, Figure 3A), indicating that binding of isoniazid by the first subunit of the homodimer affects binding to the second.

The data also indicate that there are fundamental differences between the wild-type KatG and KatG(S315T) active sites. KatG(S315T) appears to have a lower ϵ_{Soret} and has a pronounced shoulder at 360 nm, perhaps suggesting an increase in the amount of 6-coordinate iron present. As for wild-type KatG, the heterogeneous KatG(S315T) EPR spectrum supports the presence of both 5- and 6-coordinate iron, but the ratio of each species appears to be altered. Furthermore, EPR simulations identified a species (R1) unique to KatG(S315T) with $\tilde{g}_{\text{eff}} = 6.30$, 5.14, and 2.

Importantly, although KatG(S315T) differs from wild-type KatG in its ability to recognize isoniazid as a substrate, it is still able to bind isoniazid. This conclusion is supported by changes in the T_1 values, subtle yet consistent changes in the optical spectra, and changes in the EPR spectra following isoniazid addition. The ability of isoniazid to act as a competitive inhibitor of KatG(S315T) peroxidase activity also indicates drug binding by the mutant enzyme. In fact,

[2] Protein Data Bank (Brookhaven National Laboratory) accession code for yeast cytochrome *c* peroxidase is 1ccp.

[3] Distance was determined using the molecular visualization program RasMol v.2.5 (Biomolecular Structure Department, Glaxo Research and Development, Middlesex, U.K.).

within the error of the measurements, ^{1}H NMR relaxation measurements indicate that KatG(S315T) binds isoniazid at a distance from the heme iron equivalent to that of wild-type KatG. However, the finding of equivalent binding distances must be viewed with caution since they do not guarantee that isoniazid binds in an identical orientation in both enzymes. Since the ring protons of isoniazid are symmetrical, the relaxation times for a pair of protons (H_α or H_β) is a composite of the individual protons whose positions could differ by several angstroms (corresponding to the interproton distance across the ring) relative to the heme iron. Indeed, subtle differences in isoniazid-bound active site configurations of both enzymes are suggested by the definite differences in the optical difference spectra. In contrast to wild-type KatG, the titration of KatG(S315T) with isoniazid resulted in a featureless optical difference spectrum, suggesting that isoniazid binding does not cause a change in the coordination state of the KatG(S315T) iron. Furthermore, a double titration of KatG(S315T) with isoniazid followed by cyanide produced a type II difference spectrum of equal magnitude to that of cyanide alone, again indicating that isoniazid is unable to displace a sixth ligand present in the mutant enzyme.

Taken together, these findings suggest two possible explanations for the diminished turnover of isoniazid by KatG(S315T). One possibility is that isoniazid binds in an equivalent position and orientation in both enzymes, but the availability of the active site iron is reduced in KatG(S315T), perhaps by a more strongly coordinated sixth ligand that precludes efficient activation of the heme iron prior to isoniazid oxidation. We view this possibility less favorably, however, since KatG(S315T) retains nearly wild-type levels of catalase and peroxidase activity, indicating that the heme iron of the mutant is readily able to form the catalase−peroxidase compound I. A second possible explanation is that KatG(S315T) exhibits subtle differences from wild-type KatG in isoniazid binding (e.g., *slightly* more distant from the active site, in an altered conformation/orientation, etc.) that are outside the limits of the T_1 distance measurements. Proof of this hypothesis may have to await crystal structures of wild-type KatG and KatG(S315T), but it is interesting to consider the position of the S315 residue relative to the isoniazid distance from the heme periphery. Heym et al. modeled the KatG structure using the X-ray coordinates for yeast CCP (*19*). In that model, CCP residue S185 (analogous to S315 in KatG) lies within 2.6 Å of the heme periphery forming a hydrogen bond to the 'outer' propionate group of the heme.[2] It is therefore tempting to speculate that isoniazid binds near the S315T residue and that addition of a single methyl group from the mutant threonine residue causes subtle steric effects on isoniazid binding, which in turn impacts isoniazid oxidation. The KatG(S315T) mutation may therefore result in a nonoptimal alignment for electron transfer to isoniazid.

In summary, the seemingly conservative serine-to-threonine mutation provides maximum benefit to *M. tuberculosis* by reducing isoniazid activation while allowing retention of substantial catalase−peroxidase activity. While isoniazid turnover (and activation) likely involves a multistep reaction mechanism, altered binding of isoniazid provides a possible explanation for resistance exhibited by *M. tuberculosis* with the KatG(S315T) mutation. Additional spectroscopic and structural studies are ongoing to further define the nature of the sixth ligand and the residue(s) responsible for binding this important antibiotic in the wild-type and mutant enzymes.

ACKNOWLEDGMENT

The authors thank Whyte G. Owen for helpful discussion of the optical and kinetic data and Frank R. Cockerill, Bruce C. Kline, and James R. Uhl for many stimulating general discussions on this research. In addition, we would like to thank Slobodan I. Macura, Nenad Juranic, and Prasanna K. Mishra of the Mayo Nuclear Magnetic Resonance facility for helpful discussions and technical assistance with the relaxation time measurements. The authors also acknowledge the reviewers of the manuscript for helpful comments and for suggesting the NMR relaxation measurements.

SUPPORTING INFORMATION AVAILABLE

Figures are provided that (a) demonstrate the temperature dependence of T_{1obs} and (b) compare the wild-type KatG and KatG(S315T) EPR spectra with their composite simulated spectra (3 pages). Ordering information is given on any current masthead page.

REFERENCES

1. World Health Organization. (1996) *World Health Report*.
2. Riley, L. W. (1996) in *Tuberculosis* (Rom, W. N., and Garay, S., Eds.) pp 763−771, Little, Brown & Co., Boston, MA.
3. Zhang, Y., Heym, B., Allen, B., Young, D., and Cole, S. (1992) *Nature 358*, 591−593.
4. Zhang, Y., Garbe, T., and Young, D. (1993) *Mol. Microbiol. 8*, 521−524.
5. Connell, N. D., and Nikaido, H. (1994) in *Tuberculosis: Pathogenesis, Protection, and Control* (Bloom, B. R., Ed.) pp 333−352, ASM Press, Washington, DC.
6. Banerjee, A., Dubnau, E., Quemard, A., Balasubramanian, V., Um, K. S., Wilson, T., Collins, D., deLisle, G., and Jacobs, W. R., Jr. (1994) *Science 263*, 227−230.
7. Mdluli, K., Sherman, D. R., Hickey, M. J., Kreiswirth, B. N., Morris, S., Stover, C. K., and Barry, C. E., III. (1996) *J. Infect. Dis. 174*, 1085−1090.
8. Mdluli, K., Slayden, R. A., Zhu, Y., Ramaswamy, S., Pan, X., Mead, D., Crane, D. D., Musser, J. M., and Barry, C. E., III. (1998) *Science 280*, 1607−1610.
9. Johnsson, K., and Schultz, P. G. (1994) *J. Am. Chem. Soc. 116*, 7425−7426.
10. Rozwarski, D. A., Grant, G. A., Barton, D. H. R., Jacobs, W. R., Jr., and Sacchettini, J. C. (1998) *Science 279*, 98−102.
11. Johnsson, K., Froland, W. A., and Schultz, P. G. (1997) *J. Biol. Chem. 272*, 2834−2840.
12. Devi, B. G., Shaila, M. S., Ramakrishnan, T., and Gopinathan, K. P. (1975) *Biochem. J. 149*, 187−197.
13. Diaz, G. A., and Wayne, L. A. (1974) *Am. Rev. Respir. Dis. 110*, 312−319.
14. Marcinkeviciene, J. A., Magliozzo, R. S., and Blanchard, J. S. (1995) *J. Biol. Chem. 270*, 22290−22295.
15. Zabinski, R. F., and Blanchard, J. S. (1997) *J. Am. Chem. Soc. 119*, 2331−2332.
16. Magliozzo, R. S., and Marcinkeviciene, J. A. (1997) *J. Biol. Chem. 272*, 8867−8870.
17. Magliozzo, R. S., and Marcinkeviciene, J. A. (1996) *J. Am. Chem. Soc. 118*, 11303−11304.
18. Wang, J.-Y., Burger, R. M., and Drlica, K. (1998) *Antimicrob. Agents Chemother. 42*, 709- 711.
19. Heym, B., Alzari, P. M., Honoré, N., and Cole, S. T. (1995) *Mol. Microbiol. 15*, 235−245.

20. Musser, J. M., Kapur, V., Williams, D. L., Kreiswirth, B. N., van Soolingen, D., and van Embden, J. D. A. (1996) *J. Infect. Dis. 173*, 196−202.
21. Victor, T. C., Pretorius, G. S., Felix, J. V., Jordaan, A. M., van Helden, P. D., and Eisenach, K. D. (1996) *Antimicrob. Agents Chemother. 40*, 1572.
22. Uhl, J. R., Sandhu, G. S., Kline, B. C., and Cockerill, F. R., III. (1996) in *PCR Protocols for Emerging Infectious Diseases* (Persing, D., Ed.) pp 144−149, ASM Press, Washington, DC.
23. Wengenack, N. L., Uhl, J. R., St. Amand, A. L., Tomlinson, A. J., Benson, L. M., Naylor, S., Kline, B. C., Cockerill, F. R., III, and Rusnak, F. (1997) *J. Infect. Dis. 176*, 722−727.
24. Bradford, M. M. (1976) *Anal. Biochem. 72*, 248−254.
25. Fiamingo, F. G., Brill, A. S., Hampton, D. A., and Thorkildsen, R. (1989) *Biophys. J. 55*, 67−77.
26. Palmer, G. (1985) *Biochem. Soc. Trans. 13*, 548−560.
27. Harris, R. K. (1986) in *Nuclear Magnetic Resonance Spectroscopy*, p 82, John Wiley Publishers, New York.
28. Sakurada, J., Takahashi, S., and Hosoya, T. (1986) *J. Biol. Chem. 261*, 9657−9662.
29. Modi, S., Paine, M. J., Sutcliffe, M. J., Lian, L.-Y., Primrose, W. U., Wolf, C. R., and Roberts, G. C. K. (1996) *Biochemistry 35*, 4540−4550.
30. Solomon, I. (1955) *Phys. Rev. 99*, 559−565.
31. Bloembergen, N. (1957) *J. Chem. Physiol. 27*, 572−573.
32. Wüthrich, K. (1986) in *NMR of Proteins and Nucleic Acids*, p 27, John Wiley Publishers, New York.
33. Burns, P. S., Williams, R. J. P., and Wright, P. E. (1975) *J. Chem. Soc. Chem. Commun. 1975*, 795−796.
34. Schejter, A., Lanir, A., and Epstein, N. (1976) *Arch. Biochem. Biophys. 174*, 36−44.
35. Stone, J. R., Sands, R. H., Dunham, W. R., and Marletta, M. A. (1996) *Biochemistry 35*, 3258−3262.
36. Sutherland, G. R. J., Schick Zapanta, L., Tien, M., and Aust, S. D. (1997) *Biochemistry 36*, 3654−3662.
37. Hildebrand, D. P., Tang, H.-L., Luo, Y., Hunter, C. L., Smith, M., Brayer, G. D., and Mauk, A. G. (1996) *J. Am. Chem. Soc. 118*, 12909−12915.
38. Yonetani, T., and Anni, H. (1987) *J. Biol. Chem. 262*, 9547−9554.
39. Youn, H.-D., Yim, Y.-I., Kim, K., Hah, Y. C., and Kang, S.-O. (1995) *J. Biol. Chem. 270*, 13740−13747.
40. Lukat, G. S., Rodgers, K. R., Jabro, M. N., and Goff, H. M. (1989) *Biochemistry 28*, 3338- 3345.
41. Ikeda-Saito, M., Hori, H., Andersson, L. A., Prince, R. C., Pickering, I. J., George, G. N., Sanders, C. R., II, Lutz, R. S., McKelvey, E. J., and Mattera, R. (1992) *J. Biol. Chem. 267*, 22843−22852.
42. Emptage, M. H., Zimmermann, R., Que, L., Jr., Münck, E., Hamilton, W. D., and Orme- Johnson, W. H. (1977) *Biochim. Biophys. Acta 495*, 12−23.
43. Wever, R., and Bakkenist, A. R. J. (1980) *Biochim. Biophys. Acta 612*, 178−184.
44. Blumberg, W. E., Peisach, J., Wittenberg, B. A., and Wittenberg, J. B. (1968) *J. Biol. Chem. 243*, 1854−1862.
45. Bosshard, H. R., Anni, H., and Yonetani, T. (1991) in *Peroxidases in Chemistry and Biology* (Everse, J., Everse, K. E., and Grisham, M. B., Eds.) pp 51−84, CRC Press, Boca Raton, FL.
46. Bogumil, R., Maurus, R., Hildebrand, D. P., Brayer, G. D., and Mauk, A. G. (1995) *Biochemistry 34*, 10483−10490.
47. Bujons, J., Dikiy, A., Ferrer, J. C., Banci, L., and Mauk, A. G. (1997) *Eur. J. Biochem. 243*, 72−84.
48. McMillan, K., and Masters, B. S. S. (1993) *Biochemistry 32*, 9875−9880.
49. Critchlow, J. E., and Dunford, H. B. (1972) *J. Biol. Chem. 247*, 3714−3725.
50. Schenkman, J. B., Remmer, H., and Estabrook, R. W. (1967) *Mol. Pharmacol. 3*, 113−123.
51. Crane, B. R., Arvai, A. S., Ghosh, D. K., Wu, C., Getzoff, E. D., Stuehr, D. J., and Tainer, J. A. (1998) *Science 279*, 2121−2126.
52. Pufahl, R. A., and Marletta, M. A. (1993) *Biochem. Biophys. Res. Commun. 193*, 963−970.
53. Schenkman, J. B., and Sato, R. (1968) *Mol. Pharmacol. 4*, 613−620.

BI982023K